



Enhancing iris template matching with the optimal path method

Vladimir Novik¹ · Ivan Matveev² · Igor Litvinchev²

Published online: 29 November 2018
© Springer Science+Business Media, LLC, part of Springer Nature 2018

Abstract

Iris recognition provides a way to obtain a unique biometry-based digital key, which cannot be lost or forgotten. The accuracy of iris matching is strongly affected by correctness of alignment of its local features. It is proposed to split the matched images into several segments, then the alignment is sought using the method of the optimal path. The influence of the number of segments and restrictions on the mobility of neighboring segments on the recognition accuracy is investigated. Computational experiments were carried out with ICE2005 and CASIA databases.

Keywords Biometric identification · Iris recognition · Optimal path

Mathematics Subject Classification 68U10 · 92C55

1 Introduction

Security of connection and identity management is one the challenges in networking [11]. Biometrics provide a way to obtain a “key”, which cannot be lost or forgotten. Currently iris recognition is the most precise biometric modality among user-friendly and non-intrusive methods. Moreover, a well-grounded approach to get a quality digital key from iris is proposed [7]. Hence the development of even more precise iris identification methods is actual.

Iris identification involves selection of an annular region of eye image enclosed between the pupil and the sclera and comparison of two such regions for a pair of images. It is generally accepted to transform the iris annular region from the original image to a rectangle of specified size (*normalization*). Of all possible ways of normalization, the so-called “rubber-sheet” model proposed in [3] is the most

popular and, apparently, close to optimal. Here we will be within this framework.

As a rule, the texture of the iris is uniform throughout its area, but it has a large number of small details. For this reason, the most successful matching methods are based on a comparison of the local texture characteristics, which are calculated by spatially and spectrally local transformations, such as Gabor or LoG wavelets. This approach was proposed already in the earliest papers [4, 23]. Many other types of features and methods of their matching, developed since then, are also essentially local, for example the key points of the iris [25], ordinal statistics [20], correlators [16]. The use of global descriptors such as PCA, LDA or ICA [5, 22], histograms [10], Fourier transforms [15], and a number of others [1, 2] did not justify itself. All these methods show the recognition error of $EER \geq 1\%$, which is significantly worse than that of local methods, or their results are obtained on small and specific image bases.

The use of local characteristics for matching requires the alignment of the matched objects, preferably as accurate as possible. The inaccuracy in determining the iris region by the border detection algorithms is a big problem, since it generates nonlinear distortions.

Figure 1 schematically shows the results of the normalization of the initial image (a) with correctly calculated boundaries (b), with a relative error of 10% of the radius of the pupil (c) and a relative error of 10% in determining the radius of the iris (d). It is easy to see that the deformation has a regular character. However, an accurate (analytical)

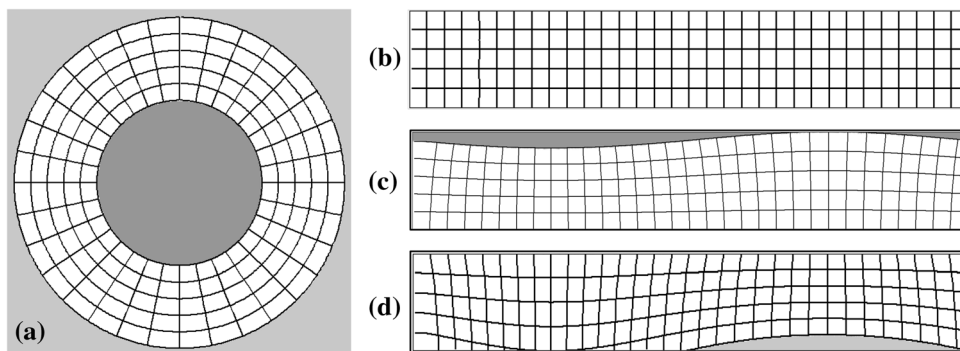
The authors would like to appreciate the opportunity to present the results at COMPSE 2018, Bangkok, Thailand. The work is supported by the Russian Foundation of Basic Research, Project No. 16-51-55019.

✉ Ivan Matveev
matveev@ccas.ru
Vladimir Novik
novikvp@mail.ru

¹ Iritech Inc., 21, B.Tatarskaya, Moscow, Russia 115184

² FRC CSC RAS, 40, Vavilov str., Moscow, Russia 119333

Fig. 1 Distortions of normalized image



description is rather difficult, since it requires the account of at least four parameters, which can be determined inaccurately (two coordinates of the eye center and two radii of circles approximating the inner and outer boundaries of the iris). For more accurate iris models, the number of parameters increases, for example, for a model of two nonconcentric circles, there are six parameters. This problem is poorly conditioned and its solution is practically inapplicable due to instability. Therefore, heuristic ways of matching are investigated mainly.

The main heuristic is the understanding that these distortions change the local texture weakly, so the similarity of local areas is preserved. Considering this, templates should be matched through a set of their local areas, some area from the first template should find its vis-a-vis in the second template with some offset, and the offsets for different pairs of areas should not be necessarily equal. In this formulation, the main issue is what kind of offsets this can be and how they are related to each other for different areas. In [12] the case of unbound offsets is considered, which are then combined using the hidden Markov model. In [25] the calculation of nonlinear deformations of the iris is carried out by tracking the corresponding points using a special kind of correlator. In [13] global (to compensate for the angle of view) and local (to compensate for the inaccuracy in determining the pupil and iris) corrections are proposed. In [17, 19, 21] neighboring areas are aligned by elastic graphs. These methods are quite computationally complex. In this paper we propose a simpler approach based on the calculation of the optimal path.

The following section briefly describes the procedure for converting an eye image to a template. Then the application of optimal path to template matching is presented. The last section describes the statement of the computational experiment, its results and conclusions.

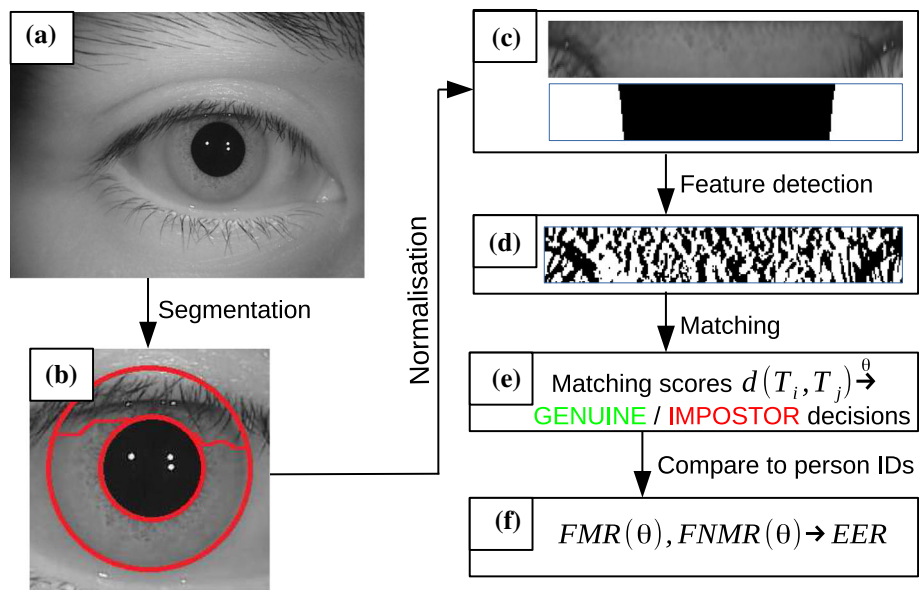
2 Making template out of image

Consider a test database containing a set of eye images. Images are labelled with the persons' unique identifiers in order to verify the correctness of identification. There is more than one person in the database and more than one image per person. The basic processing scheme is depicted in Fig. 2. Here blocks represent the “state of the world” and are labelled with Latin chars as: source image (a), segmentation (b), normalized image and mask (c), extracted features forming the template (d), cross-matching decisions (e), and matching statistics and aggregated error values (f). Arrows represent the processes, which transform a state to the next one.

Source image $I(x, y)$ is segmented by method [6], which outputs the segmentation results as pupil contour, iris contour and occlusion mask. The pupil contour is the circle given by its center and radius (x_p, y_p, r_p) , which is the best approximation of pupil-iris boundary. The iris contour is the circle (x_I, y_I, r_I) , approximating iris-sclera boundary. The occlusion mask $M(x, y)$ is an image of same size as source with zero pixels in place where iris is covered by eyelids, eyelashes, flashes etc.

Then the *iris normalisation* is performed. It is a mapping of a ring, enclosed between iris and pupil circles to a rectangular region. The normalized image coordinate system is rectilinear $O\phi\rho$, where horizontal axis $O\phi$ corresponds to angle measured along the pupil and iris circles in source image, and vertical axis $O\rho$ corresponds to radial shift from pupil circle to iris circle. Both source image and mask are subjected to the transformation, which yields their normalized versions $I(\phi, \rho)$ and $M(\phi, \rho)$. Figure 2c depicts a sample of normalized image obtained from image in Fig. 2(a) and occlusion mask thereof. There are several possible models of this transformation, here the so called “rubber-sheet model” [3] is used. The origin (x, y) for the point of normalised image (ϕ, ρ) is expressed as:

Fig. 2 The processing scheme



$$\begin{aligned}
 x(\phi, \rho) &= (1 - \rho)x_1(\phi) + \rho x_2(\phi), \\
 x_1(\phi) &= x_P + r_P \cos(\phi), \\
 x_2(\phi) &= x_I + r_I \cos(\phi),
 \end{aligned}
 \tag{1}$$

Coordinate y is computed accordingly. Dimensions of normalized image are set in ranges: $\rho \in [0; 1]$, $\phi \in [0; 2\pi)$. Brightness of the normalized image is obtained with the bilinear interpolation:

$$\begin{aligned}
 N(\phi, \rho) &= (1 - \{x\})(1 - \{y\})I(\lfloor x \rfloor, \lfloor y \rfloor) \\
 &+ \{x\}(1 - \{y\})I(\lfloor x \rfloor + 1, \lfloor y \rfloor) \\
 &+ (1 - \{x\})\{y\}I(\lfloor x \rfloor, \lfloor y \rfloor + 1) \\
 &+ \{x\}\{y\}I(\lfloor x \rfloor + 1, \lfloor y \rfloor + 1),
 \end{aligned}
 \tag{2}$$

where $\lfloor a \rfloor$ and $\{a\}$ are integer and fractional parts of a respectively.

Iris features $V(\phi, \rho)$ are calculated as convolution of normalized image (2) with Gabor filter:

$$\begin{aligned}
 V(\phi, \rho) &= N(\phi, \rho) * g_{\sigma\lambda}(\phi, \rho), \\
 g_{\sigma\lambda}(\phi) &= \exp\left(-\frac{\phi^2}{2\sigma^2}\right) \exp\left(-i\frac{\phi}{\lambda}\right),
 \end{aligned}
 \tag{3}$$

where σ and λ determine the spread of the wavelet in spatial domain and the wavelength of modulation. It should be noted that 1D Gabor (3) wavelet is used, where dimension spans along the angular coordinate ϕ . To form 2D functions one might multiply spatial representations of the filters by delta function $\delta(r)$. Finally, the features used for matching are obtained as binarization of real and imaginary parts of array $V(\phi, \rho)$:

$$\begin{aligned}
 T_{Re}(\phi, \rho) &= \begin{cases} 1, & \Re(\mathfrak{B}(\phi, \rho)) > \theta, \\ 0, & \text{otherwise,} \end{cases} \\
 T_{Im}(\phi, \rho) &= \begin{cases} 1, & \Im(\mathfrak{B}(\phi, \rho)) > \theta, \\ 0, & \text{otherwise,} \end{cases}
 \end{aligned}
 \tag{4}$$

Two components of (4) are joined together to form a template. In this work binary templates are used in experiments. But without loss of generality one can speak about any system of local features, which are calculated in a regular mesh. So, each eye image $I(x, y)$ is converted to a template $T(\phi, \rho)$ and accompanying mask $M(\phi, \rho)$.

3 Template matching

Any two binary templates can be matched with normalized Hamming distance:

$$d_0(T_1, T_2) = \frac{1}{|\Omega|} \sum_{(\phi, \rho) \in \Omega} T_1(\phi, \rho) \oplus T_2(\phi, \rho),
 \tag{5}$$

where $\Omega = M_1 \cap M_2$ is the intersection of non-occluded areas of two matching templates. In fact, more complex distance function should be used, which counts on possible uncertainty of iris angle due to image rotation. The rotation of source eye image turns to cyclic shift along ϕ coordinate in normalized image. One of the templates (together with mask) is rotated and matched, minimum distance is found:

$$\begin{aligned}
 d(T_1, T_2) &= \min_{\psi \in [-S; S]} d(T_1, T_2, \psi), \\
 d(T_1, T_2, \psi) &= \frac{1}{\Omega(\psi)} \sum_{(\phi, \rho) \in \Omega} T_1(\phi + \psi, \rho) \oplus T_2(\phi, \rho) \\
 \Omega(\psi) &= M_1(\phi + \psi) \cap M_2(\phi),
 \end{aligned} \tag{6}$$

where ψ is a possible rotation limited by maximum allowed rotation angle S of tested iris. The distance is normalized to the range $[0; 1]$.

Let's now split the template T_1 into N equally sized, non-intersecting, fully covering segments $T_1^{(n)}$, $n \in [1; N]$, which are located along angular axis as shown in Fig. 3. Each such segment may be displaced by some angle $\psi_n \in [-S; S]$ and matched against corresponding part of T_2 template according to (5). Partial distances obtained here can be organized as the matrix $D = \{d_{\psi,n}\}$ with size $(2S + 1) \times N$. Note that the computational complexity of obtaining this matrix does not exceed that of determining the distance (6). In these terms, the distance (6) is obtained as the minimum sum over the rows of the matrix D :

$$d(T_1, T_2) = \min_{\psi} \sum_n d_{\psi,n}. \tag{7}$$

That is, the angular displacements of all segments are the same, which can be called as a model of a non-deformed “rigid body”. On the other hand, angular displacements can be made independent, minimizing each partial distance separately:

$$d(T_1, T_2) = \sum_n \min_{\psi} d_{\psi,n}. \tag{8}$$

This corresponds to a model of a body, perfectly elastic with respect to rotations. A computational experiment with independent template displacements was carried out as described below. The model (8) gives a lesser identification error than (7) in conditions of inaccuracy of border detection when number of segments is small: $2 \leq N \leq 6$. As the number of segments increases, the error increases due to locating false matches for small segments. The question arises whether it is possible to improve the

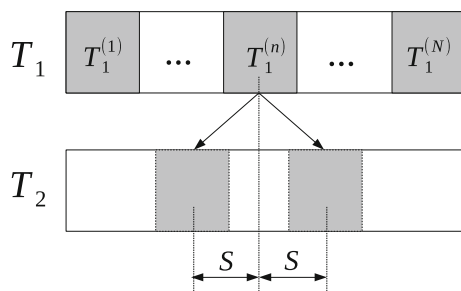


Fig. 3 Matching segments with angular shift

alignment, if we introduce some restrictions on the mutual motion of segments. So, the nature of template should be something between completely restricted “rigid” body (7) and completely unconstrained (by angle) model (8). In this situation, in [12] it is proposed to make a relationship between displacements by introducing a hidden Markov chain. In this paper, we propose to use the optimal path method.

The smoothness of the normalization transformation means that the values ψ_n for neighboring indices are close. Values for distant indexes can vary greatly, but because of the cyclicity of the angle conversion, the values of ψ_1 and ψ_N should also be close. Thus, we get the task of selecting a sequence of elements of matrix $\{d_{\psi,n}\}$, with the following requirements: one and only one element in each column; row of selected elements changes no more than by small value between adjacent columns; sum of the selected elements is minimized. It is possible to present this problem as the definition of the minimum cost of a cyclic path in a matrix:

$$\begin{aligned}
 d(T_1, T_2) &= \min_{(\psi_1, \dots, \psi_N)} \sum_{n=1}^N [d_{\psi,n} + C(\psi_n, \psi_{n+1})], \\
 C(\psi_n, \psi_{n+1}) &= \begin{cases} 0, & \text{if } \|\psi_n - \psi_{n+1}\| \leq 1, \quad n \neq N, \\ 0, & \text{if } \|\psi_1 - \psi_N\| \leq 1, \quad n = N, \\ \infty, & \text{otherwise.} \end{cases}
 \end{aligned} \tag{9}$$

The problem (9) is an optimization of path on a grid, which can be solved by various methods [24]. Figure 4 represents typical view of matrices D for three cases and the optimal path found. The size of the matrices is $N = 15$, $S = 12$. The darker is the cell the smaller partial distance is. The optimal path is outlined with white circles. First matrix (a) is the case of matching two irises of one person (i.e. “genuine” match), when all border parameters are detected correctly (or, maybe, have very similar errors). In this case no rotation is necessary, optimal path is a straight line and “rigid body” model would suffice as well. Matrix (b) is the case of genuine matcher, but normalization is distorted by border detection error. Here one can see that minima in columns appear in some regular order, which forms a dark “valley”, and the optimal path is a curved path through it. Matrix (c) is a case of impostor match. Would it be correct border detection or not, matrix of impostor match will have chaotic location of minima in its columns, and the optimal path will be forced through many large values of matrix, yielding high total cost. The solution of (9) produces the distance and the angles (ψ_1, \dots, ψ_N) , to which the template segments are offset to find their correspondents.

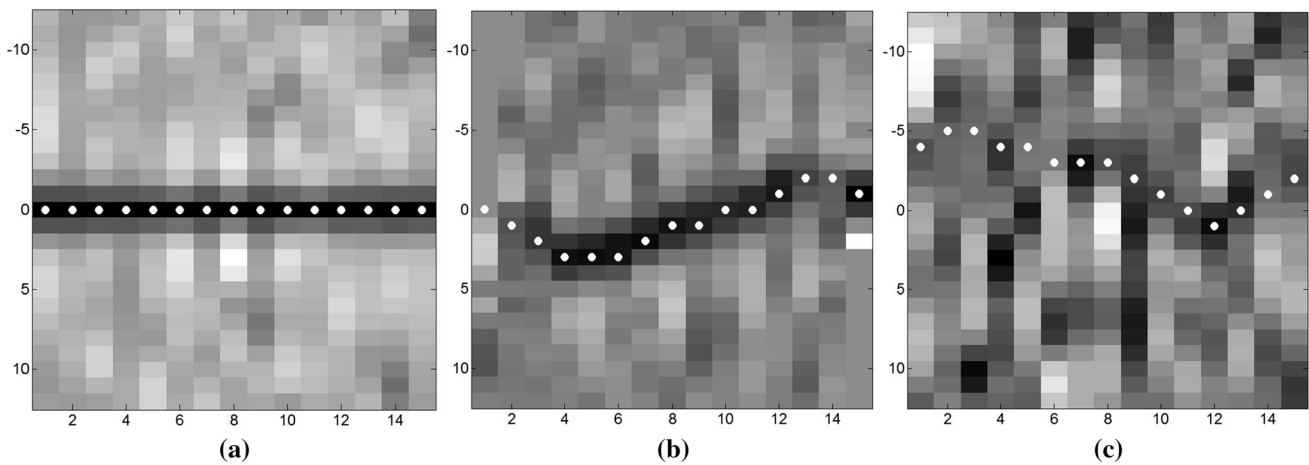


Fig. 4 Matrices D for undistorted, distorted genuine and impostor matches

In all the calculations of this section an arbitrary parameter N is used, the number of segments to which the template is divided. The selection of this parameter was carried out experimentally, by calculating the classification error obtained by using the distance with the given parameter N .

4 Experiment setup and results

By adding a threshold $\Theta \in (0; 1)$ to the distance $d(T_1, T_2)$ the classifier is obtained:

$$Class = \begin{cases} \text{genuine}, & \text{if } d(T_1, T_2) \leq \Theta, \\ \text{impostor}, & \text{if } d(T_1, T_2) > \Theta. \end{cases} \quad (10)$$

Since the persons’ unique identifiers are known for test database, the decision of classifier can be matched against the ground truth, and the quality of classifier can be evaluated from the number of wrong classification events. The equal error rate is defined by a trade-off between false match and false non-match errors, which is governed by a classification threshold Θ :

$$EER \equiv \frac{fn(\Theta)}{fn(\Theta) + tp(\Theta)} = \frac{fp(\Theta)}{fp(\Theta) + tn(\Theta)}, \quad (11)$$

where $fn(\Theta)$, $fp(\Theta)$ are numbers of false non-match and false match events (also referred to as false negative and false positive), and $tn(\Theta)$, $tp(\Theta)$ are true non-match and true match numbers respectively. As long as EER depends on number of template segments, one can think of it as a function $EER(N)$ and search for the optimum:

$$EER^* = \min_N EER(N), \quad N^* = \arg \min_N EER(N). \quad (12)$$

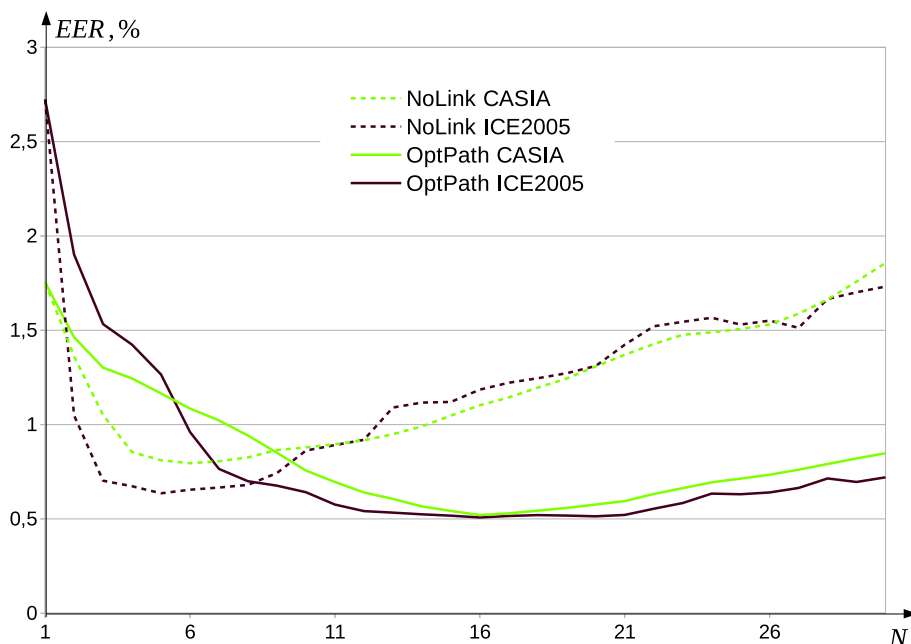
Two publicly available iris image databases were used: ICE2005 subset of ND-Iris-0405 [18] and CASIA4-Lamp [9]. All images in the datasets are 480 rows and 640

columns. ICE2005 subset contains 2593 images for 132 persons. Majority of the subjects are Caucasian. All images were acquired with LG 2200 iris biometrics system. The subset of all left irises including 1527 images of 119 persons was used for experiments. Number of images per iris is very uneven in this database and ranges from single (33 persons have only one image) to 31. Number of genuine matches is 15, 357, number of impostor matches is 1, 149, 744. CASIA4-Lamp contains images for over 800 irises, each iris is represented by 20 or rarely a couple less images. Totally, the DB contains 16, 312 images All irises are Asian type. Images were collected in near-infrared illumination using IKEMB-100 camera produced by OKI-IrisPass (<http://www.oki.com>). This produces approximately $800 * 20 * 20 / 2 = 160$ k genuine matches and $16,312^2 / 2 - 160,000 \approx 13$ M impostor matches.

Figure 5 presents graphs of dependency of EER on the number of segments N , $N \in [1; 30]$ for two involved databases. Graphs, which are entitled “NoLink”, are obtained for model of unrelated segments and distance (8), graphs “OptPath” are derived for optimal path model with distance (9). Note that the initial points of these graphs $N = 1$ coincide and correspond to the “rigid body” model (7).

Based on the graphs, the following conclusions can be drawn. The model of a “rigid body” almost always loses to models with division into segments. Models with unrelated segments for a small number of segments are better than models of the optimal path, but with an increase in the number of segments, they quickly saturate and further their error increases. Models of the optimal path are saturated more slowly, but they achieve substantially better results. Comparing databases (ICE2005 against CASIA), one can see that at $N = 1$ ICE2005 yields bigger EER value, but with growing N it allows better classification for both matchers. The reason is ICE2005 has bigger share of images with low quality, which produce imprecise border

Fig. 5 Graphs of EER(N) for various databases and matchers



detection and template matching error with “rigid body” method. On the other hand, ICE2005 has more diversified iris types and in general less occlusions; both of these factors allow achieving better precision if border detection error influence is compensated.

The Table 1 gives the EER (11) in percent for proposed approach and some state of the art methods for two databases involved.

“Rigid body”, which is a straightforward implementation of Daugman’s scheme [4] has poor performance and loses to any of state of the art approaches. Splitting into segments and unconstrained matching (8) enhances the situation substantially, but still is inferior to other methods. The optimal path model covers the gap, and the proposed method demonstrates same recognition quality as known solutions according to EER. At that optimal path method is quite simple both algorithmically and computationally.

Table 1 EER for various methods

Method	ICE2005	CASIA
Zhang et al. [25]	–	0.59
Liu et al. [14]	0.63	–
He et al. [8]	0.53	–
Rigid body, $N = 1$	2.72	1.76
Nolink, optimal $N = 5$	0.64	0.79
Optimal path, optimal $N = 16$	0.52	0.54

5 Conclusions

The influence of splitting the iris into the segments upon classification error was studied. The models of “rigid body”, unconstrained segment offset and alignment by optimal path were investigated. Numerical experiments have shown that this algorithm can significantly improve the accuracy of recognition and achieve the performance of complex state of the art approaches. The highest accuracy is achieved with five segments for unconstrained offset model and 16 for optimal path model. The running time of the algorithm with $N = 16$ is 150 microseconds per one comparison with Intel Core i7-3770 CPU and allows for multiple acceleration when using multiprocessor systems.

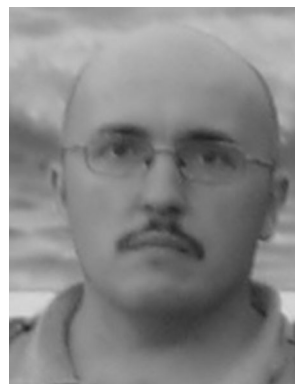
References

1. Bowyer, K., Hollingsworth, K., & Flynn, P. (2013). A survey of iris biometrics research: 2008–2010. In M. J. Burge & K. W. Bowyer (Eds.), *Handbook of iris recognition, advances in computer vision and pattern recognition* (pp. 15–54). London: Springer. <https://doi.org/10.1007/978-1-4471-4402-1-2>.
2. Bowyer, K. W., Hollingsworth, K., & Flynn, P. J. (2008). Image understanding for iris biometrics: A survey. *Computer Vision and Image Understanding*, 110(2), 281–307. <https://doi.org/10.1016/j.cviu.2007.08.005>.
3. Daugman, J. (2002). How iris recognition works. *Proceeding International Conference on Image Processing, I*, I-33–I-36.
4. Daugman, J. G. (1993). High confidence visual recognition of persons by a test of statistical independence. *IEEE Transactions on Pattern Analysis and Machine Intelligence*, 15(11), 1148–1161.

5. Erbilek, M., & Toygar, O. (2009). Recognizing partially occluded irises using subpattern-based approaches. In *2009 24th international symposium on computer and information sciences* (pp. 606–610). <https://doi.org/10.1109/ISCIS.2009.5291890>
6. Gankin, K., Gneushev, A., & Matveev, I. (2014). Iris image segmentation based on approximate methods with subsequent refinements. *Journal of Computer and Systems Sciences International*, 53(2), 224–238.
7. Hao, F., Anderson, R., & Daugman, J. (2006). Combining crypto with biometrics effectively. *IEEE Transactions on Computers*, 55(9), 1081–1088. <https://doi.org/10.1109/TC.2006.138>.
8. He, Z., Tan, T., Sun, Z., & Qiu, X. (2009). Toward accurate and fast iris segmentation for iris biometrics. *IEEE Transactions on Pattern Analysis and Machine Intelligence*, 31(9), 1670–1684.
9. Institute of Automation, Chinese Academy of Sciences: CASIA Iris Image Database (2010). <http://biometrics.idealtest.org/>.
10. Ives, R. W., Guidry, A. J., & Etter, D. M. (2004). Iris recognition using histogram analysis. In *Conference record of the thirty-eighth asilomar conference on signals, systems and computers, 2004*, (Vol. 1, pp. 562–566). <https://doi.org/10.1109/ACSSC.2004.1399196>
11. Jing, Q., Vasilakos, A. V., Wan, J., Lu, J., & Qiu, D. (2014). Security of the internet of things: Perspectives and challenges. *Wireless Networks*, 20(8), 2481–2501. <https://doi.org/10.1007/s11276-014-0761-7>.
12. Kerekes, R., Balakrishnan, N., Thornton, J., Savvides, M., & Kumar, B. V. K. V. (2007) Graphical model approach to iris matching under deformation and occlusion. In *CVPR* (pp. 1–6). IEEE Computer Society. <http://www.cs.cmu.edu/~muralib/cvprDraft.pdf>
13. Li, X. (2005). Modeling intra-class variation for nonideal iris recognition. In D. Zhang & A. Jain (Eds.), *Advances in biometrics, lecture notes in computer science* (Vol. 3832, pp. 419–427). Heidelberg: Springer. <https://doi.org/10.1007/11608288-56>.
14. Liu, J. (2011). A novel image deblurring method to improve iris recognition accuracy. In *IEEE international joint conference on biometrics* (pp. 1–8)
15. Miyazawa, K., Ito, K., Aoki, T., Kobayashi, K., & Nakajima, H. (2005). An efficient iris recognition algorithm using phase-based image matching. In *IEEE international conference on image processing 2005* (Vol. 2, pp. II49–II52). <https://doi.org/10.1109/ICIP.2005.1529988>
16. Pavelieva, E. A. (2013). Searching for correspondences between the key points of the images of the irises of the eyes using the method of the projected phase correlation. *Systems and Means of Informatics*, 23(2), 74–88.
17. Phang, S. S., Boles, W. W., & Collins, M. J. (2006). Tracking iris surface deformation using elastic graph matching. In *Proceedings of the twenty-first international conference, image and vision computing new zealand (IVCNZ2006), Great Barrier Island, New Zealand* (pp. 3–8)
18. Phillips, P. J., Scruggs, W. T., O’Toole, A. J., Flynn, P. J., Bowyer, K. W., Schott, C. L., et al. (2010). Frvt 2006 and ice 2006 large-scale experimental results. *IEEE Transactions on Pattern Analysis and Machine Intelligence*, 32(5), 831–846.
19. Songjang, T., & Thainimit, S. (2015). Tracking and modeling human iris surface deformation. In *2015 12th International Conference on Electrical Engineering/Electronics, Computer, Telecommunications and Information Technology (ECTI-CON)* (pp. 1–5). <https://doi.org/10.1109/ECTICon.2015.7207025>
20. Sun, Z., & Tan, T. (2009). Ordinal measures for iris recognition. *IEEE Transactions on Pattern Analysis and Machine Intelligence*, 31(12), 2211–2226. <https://doi.org/10.1109/TPAMI.2008.240>.
21. Thainimit, S., Alexandre, L., & de Almeida, V. (2013). Iris surface deformation and normalization. In *2013 13th international symposium on communications and information technologies (ISCIT)* (pp. 501–506). <https://doi.org/10.1109/ISCIT.2013.6645910>.
22. Vivekanand, D., Schmid, N. A., & Fahmy, G. (2005). Performance evaluation of iris-based recognition system implementing PCA and ICA encoding techniques. In *Proceedings volume 5779, biometric technology for human identification II*. <https://doi.org/10.1117/12.604201>.
23. Wildes, R. (1997). Iris recognition: An emerging biometric technology. *Proceedings of the IEEE*, 85(9), 1348–1363.
24. Xu, J., Yang, J., Guo, C., Lee, Y. H., & Lu, D. (2015). Routing algorithm of minimizing maximum link congestion on grid networks. *Wireless Networks*, 21(5), 1713–1732. <https://doi.org/10.1007/s11276-014-0878-8>.
25. Zhang, M., Sun, Z., & Tan, T. (2011). Deformable daisy matcher for robust iris recognition. In *2011 18th IEEE international conference on image processing* (pp. 3189–3192). <https://doi.org/10.1109/ICIP.2011.6116346>



Vladimir Novik received M.Sc. degree at the Moscow Institute of Physics and Technology in 1997. Since 1997 research assistant at Moscow Design Bureau “Electron”. Since 2001 researcher and software engineer at Iritech, Inc. Research interests: image processing, biometric identification, iris recognition, remote sensing.



Ivan Matveev received the M.Sc. degree at the Moscow Institute of Physics and Technology in 1997, Ph.D. in 1999 and Dr.Sci. in 2014 from Computing Centre of Russian Academy of Sciences. Since 2004 he runs Intellectual Systems sector of the Complex Systems Department at Computing Centre of Russian Academy of Sciences. Research interests: biometric identification, face and iris recognition, realtime image processing.



Igor Litvinchev received his M.Sc. degree from Moscow Institute of Physics and Technology (Fizteh), Ph.D. and Dr. Sci. (Habilitation) degrees from Computing Center of Russian Academy of Sciences. His research focuses on large-scale systems modeling, optimization and control. In this area he published 4 books and more than 60 journal papers. He was principal investigator in more than 30 projects supported by NATO Scientific Affairs Division and European Community; ISF (USA); RFBR (Russia); CNPq

and FAPESP (Brasil); BRFB (Belarus); CONACYT, PROMEP and PAICYT (Mexico). Prof. Litvinchev is a member of Russian Academy of Natural Sciences and Mexican Academy of Sciences.